Appendix for Stringent Control Over Cytoplasmic and Membrane Densities Defines Cell Geometry in *Escherichia coli*

Griffin Chure[1], Roshali T. de Silva[1], Richa Sharma[1], Michael C. Lanz[1,2], and Jonas Cremer[1,3]

[1]Department of Biology, Stanford University, Stanford, CA, USA
[2]Chan-Zuckerberg Biohub, San Francisco, CA, USA
[3]jonas.cremer@stanford.edu

October 29, 2023

Contents

1 Approximating cytoplasmic drymass density from total drymass density **2**

2 Bayesian Inference **4**
2.1 Growth-Rate Dependent Total Protein Per Cell From Literature Data 5
2.2 Growth Rate Dependent Surface Area from Literature Data 5
2.3 Growth Rate Dependent Ribosomal Proteome Fraction from Literature Data 6
2.4 Growth-Rate Independent Inference of Total Drymass Density from Literature Data 7
2.5 Growth-Rate Independent Inference of Membrane Proteome Fraction from Literature Data 7
2.6 Growth-Rate Independent Inference of Membrane Protein Density From Literature Data . . 8
2.7 Growth-Rate Dependent Inference of Periplasmic Proteome Fraction From Literature Data . 9
2.8 Inference of RNA-to-Protein From Our Experimental Measurements 10
2.9 Inference of Membrane and Periplasmic Protein From Our Experimental Measurements . . . 10
2.10 Inference of Steady-State Growth Rates From Our Experimental Measurements 11
2.11 Inference of Cell Shape Parameters From Our Experimental Measurements 11

3 Culturing Media and Biochemical assays **14**
3.1 Culturing media 14
3.2 Quantification of Total Protein and Total RNA 14
3.3 Quantification of Total Periplasmic Protein 15
3.3.1 Overview and Control 15
3.3.2 Separation Protocol 15
3.3.3 Mass Spectrometry to Confirm Separation Assay 15
3.4 Quantification of Total Membrane Protein 17

4 Image Processing **18**

1 Approximating cytoplasmic drymass density from total drymass density

A central component of this work is the empirical observation that the total drymass density (meaning, total drymass per total cell volume) is i) constant across growth conditions and ii) approximately equal to the cytoplasmic drymass. The former is supported by measurements of total drymass densities in different studies (Fig. 1(C) of the main text), the latter is expected given that the cytoplasm accounts for most of the celluar volume and harbors most of the cellular mass. In this section we present a reanalysis of proteomics and other cellular composition data to show that the total drymass density well approximates the cytoplasmic drymass.

The total cytoplasmic density can be defined as

$$\rho_{cyt} = \frac{M_{RNA} + M_{DNA} + M_{prot}^{(cyt)} + \dots}{V_{cyt}}, \tag{1}$$

where M_{RNA} is the total RNA mass, M_{DNA} is the total DNA mass, $M_{prot}^{(cyt)}$ is the total mass of cytoplasmic protein, and the ellipsis $(\dots)$ denotes all other drymass components like metabolites. A difference from the Eq. 2 of the main text is the specification of the cytoplasmic volume V_{cyt} rather than the total cell volume, which accounts for a periplasmic volume $V_{cyt} = V_{tot} - V_{peri}$.

As DNA, RNA, and protein are the predominant components of *E. coli* drymass [1], we examined if these masses, and therefore the total cytoplasmic density, could be inferred from literature data. Specifically, we leveraged a collection of proteomic datasets [2–7] and direct measurements of the total DNA-to-protein ratio [1, 8–10].

Recently, Babu *et al.* [11] peformed a thorough survey of the *E. coli* envelope proteome. Using their gene-by-gene level classification of protein localization, we computed the total mass fraction of all cytoplasmic proteins ϕ_{cyt} as identified in the proteomic data sets. Thus, to estimate the total mass of cytoplasmic protein, we can simply perform the multiplication

$$M_{prot}^{(cyt)} = \phi_{cyt} M_{prot}^{(tot)}(\lambda), \tag{2}$$

where $M_{prot}^{(tot)}(\lambda)$ is the total protein mass per cell as a function of the growth rate. As each measurement in our collated proteomic dataset corresponds to a specific growth rate λ, this property can be computed on a per-point basis, so long as one knows how the total protein mass scales with growth rate. To generate this relation, we performed an empirical fit of an exponential function to a collection of literature measurements of total protein per cell [1, 5, 7, 8, 12, 13] [Fig. A1(A)]. Details for how this fit was performed, along with specific prior distributions used, is provided in Sec. 2.

In a similar vein, we can caluclate the total RNA mass M_{RNA} by knowing the ribosomal mass fraction of the proteome. By mass, ribosomal RNA accounts for the vast majority of all cellular RNA ($\approx 86\%$ BNID: 106421; [14, 15]). We can thus calculate the total mass of RNA from the total ribosomal content as

$$M_{RNA} = \beta \phi_{rib} M_{prot}^{(tot)}(\lambda), \tag{3}$$

where ϕ_{rib} is the proteome mass fraction of ribosomal protein and β is a conversion factor. This factor can

be calculated as

$$\beta = \frac{M_{RNA}}{M_{rRNA}} \frac{M_{rRNA}}{M_{prot}^{(rib)}} = \frac{1\,\mu g\, RNA}{0.86\,\mu g\, rRNA} \times \frac{1\,\mu g\, rRNA}{0.53\,\mu g \text{ ribosomal protein}} = 2.19 \frac{\mu g\, RNA}{\mu g \text{ protein}}, \tag{4}$$

which is also derived in the supplement of Scott *et al.* [15].

The remaining mass that we must compute is the total DNA, M_{DNA}. Literature studies [Fig. A1(B)] [8–10, 13] suggest that the relative mass of DNA to protein θ_{DNA} is i) small and ii) not strongly dependent on the the growth condition. Assuming this ratio is constant, we can calculate the total DNA mass as

$$M_{DNA} = \theta_{DNA} M_{prot}^{(tot)}(\lambda). \tag{5}$$

With Eq. 2 through Eq. 5, we have calculations in place for all of the major components of cellular drymass. As the proteomic data are not coupled with cell size measurements, however, we must further use empirical descriptions to calculate the cytoplasmic volume. In the main text, we treated the total cell volume V_{tot} to be approximately equal to the cytoplasmic volume V_{cyt}. This is a fair approximation in conditions where the total cell volume is large, but can be inadequate in cases where the total cell volume is small and the periplasm thus accounts for a larger fraction of the total cell volume. Here, we do a full accounting for this volume effect.

The periplasm of *E. coli* is on average very narrow, on the order of $\delta \approx 25$ nm [16]. As a result, the total periplasmic volume can be approximated as

$$V_{peri} = S_A \cdot \delta, \tag{6}$$

where S_A is the cell surface area. With this in hand, we can calculate the cytoplasmic volume at growth rate λ given knowledge of the surface area S_A and total volume V_{tot},

$$V_{cyt} = V_{tot}(\lambda) - \delta S_A(\lambda). \tag{7}$$

which demands empirical descriptions of V_{tot} and S_A as a function of the growth rate. For these, we assumed an exponential and linear dependence on the growth rate, respectively, which adequately described the observations [Fig. A1(C-D)]. In Section 2, we enumerate the Bayesian model used for this fitting.

Thus, with Eq. 7, we have complete parametric knowledge of Eq. 1, allowing us to estimate the cytoplasmic density at a given growth rate λ as

$$\rho_{cyt} = \frac{M_{prot}^{(tot)}(\lambda)\left[\beta\phi_{rib} + \phi_{cyt} + \theta_{DNA}\right]}{V_{tot}(\lambda) - \delta S_A(\lambda)}. \tag{8}$$

Fig. A1(E) shows this calculation for each measurement in our collated proteomic dataset (green) overlaid with the direct measurements of the total drymass (grey). We see a growth-rate independent, systematic upward shift in the cytoplasmic drymass density, though the error bars (representing the 95% credible region for each estimate) are wide. Importantly, while there is a systematic shift by $\approx$ 30-50 fg / fL, this corresponds to a 10% - 20% change in its absolute value, changing the density ratio κ by the same degree, not impacting the density theory introduced and probed in the main body of this study.

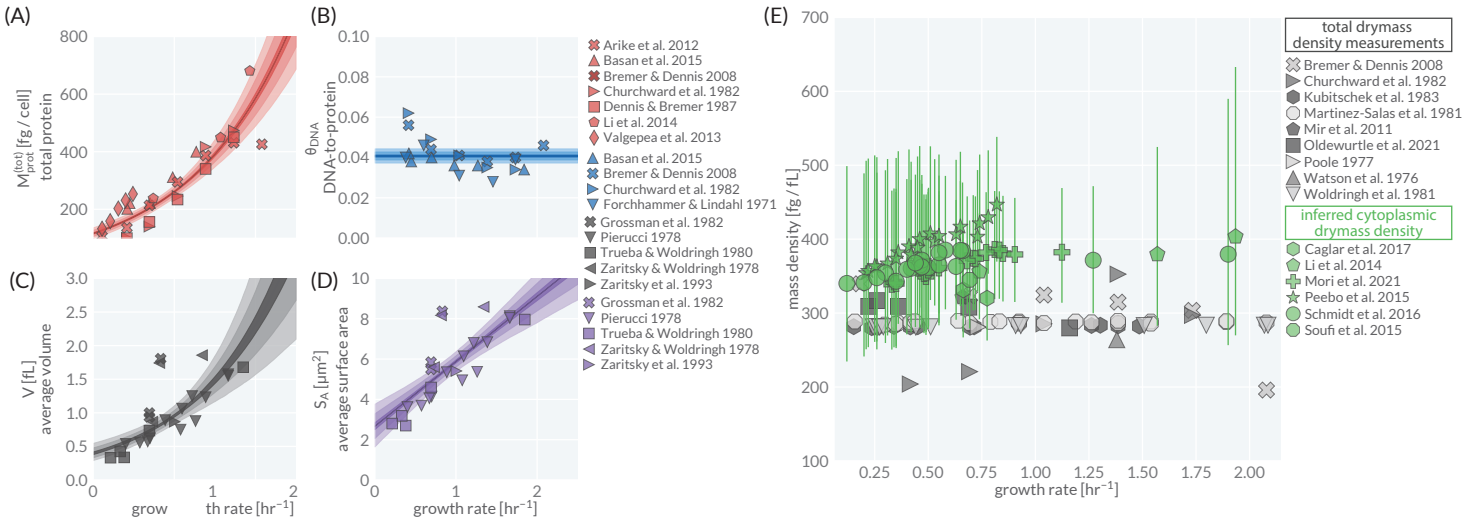

Figure A1: Comparison of measured drymass density with cytoplasmic drymass density inferred from mass spectrometry data. (A) Empirical fit of total protein as a function of the growth rate. (B) Inferred empirical constant for the DNA-to-protein ratio as a function of growth rate. (C) Empirical exponential fit of cell volume as a function of the growth rate. (D) Empirical linear fit of total cell surface area as a function of the growth rate. (E) Using empricial fits, and analysis described in this section, we computed the empirical cytoplasmic drymass density, shown in green. Error bars correspond to bounds of the 95% credible regions. Shaded regions in (A-D) correspond to the bounds of the 95%, 75%, 25%, and median percentiles of the fit from light to dark, respectively.

2 Bayesian Inference

In this work, we utilize Bayesian statistical methods to systematically propagate all uncertainty from measurements and our model assumptions to generate the final predictions and experimental data presented in this work. In the subsections that follow, we present detailed descriptions of the various components of the inference. In all cases, inferences using literature data and inferences using our suite of experimental measurements were performed independently. Further, we note that *all* inference of model parameters and calculation of estimated membrane protein densities were conducted simultaneously, resulting in a rather large posterior probability distribution that precludes complete enumeration here. However, we invite the reader to examine the full statistical inference models, which are written using the Stan probabilistic programming language [17], and which are available on the paper GitHub repository (`github.com/cremerlab/density_maintenance`). We find that these models, coupled with the inline comments, are easier to parse than a full mathematical statement.

Speaking generally, we sought to inference the probability of a parameter θ taking on a given value, conditioned on an experimental measurement y. This quantity, termed the *posterior probability distribution* $g(\theta \mid y)$ (heretofore called simply the *posterior*) can be computed using Bayes' rule,

$$g(\theta \mid y) = \frac{f(y \mid \theta) g(\theta)}{f(y)} \tag{9}$$

where g and f denote probability density functions over parameters and data, respectively. In computing the posterior, one must minimally enumerate the likelihood function $f(y \mid \theta)$ and the prior $g(\theta)$. The denominator of Eq. 9 is termed the *evidence* or the *marginalized likelihood* and represents the probability of observing a datum y irrespective of the model. For our purposes, we can treat this as a normalization

constant and neglect it. As such, Eq. 9 becomes

$$g(\theta \mid y) \propto f(y \mid \theta) g(\theta). \tag{10}$$

The likelihood function $f(y \mid \theta)$ represents the probability of observing a datum y *given* a particular value of the parameter θ. In all cases for this work, we took the likelihood to have the form of a Gaussian distribution parameterized by a mean μ and homoskedastic error σ,

$$f(y \mid \theta) = \frac{1}{\sqrt{2\pi\sigma^2}} \exp\left[-\frac{(y-\mu)^2}{2\sigma^2}\right] \Rightarrow f(y \mid \theta) \sim \text{Normal}(\mu, \sigma) \tag{11}$$

where we have introduced a short-hand notation. Asserting a Gaussian likelihood makes an assumption about how the measurements are distributed about a mean value μ, but not *what* that mean value is. The remaining subsections of this Appendix section outline how we determine what the mean value of this likelihood function is for a variety of components of our models.

Finally, we must also provide a definition of the prior distribution over the parameter $g(\theta)$. This distributions encapsulates all knowledge we have of what the true parameter value of θ might be *without* taking the observations into account. This is a critically important point and each prior choice represents the assumptions and domain expertise we employ in crafting these models. In general, we will not justify the choice of every prior distribution in this section as there are very many. However, we have listed the prior choice for each parameter discussed in the coming sections in Table 1.

2.1 Growth-Rate Dependent Total Protein Per Cell From Literature Data

In this work, we repeatedly used literature measurements of the total protein per cell to calculate various properties, including the total periplasmic protein mass and the membrane protein density. To do so, we assumed that the total protein per cell scaled exponentially with the steady-state growth rate across conditions with the form

$$M_{prot}^{(tot)} = M_{prot,0} e^{k_{prot}\lambda}. \tag{12}$$

To simplify the inference, we performed a Bayesian linear regression on the log transform of this equation as

$$\log(M_{prot}^{(tot)}) = \beta_{prot,0} + k_{prot}\lambda, \tag{13}$$

which we took to be the mean value of a Gaussian likelihood function (Eq. 11) with a homoskedastic error $\sigma_{M_{prot}^{(tot)}}$. Chosen prior distributions are provided in Table. 1. The result of the fit of this quantity is shown in Fig. A2.

2.2 Growth Rate Dependent Surface Area from Literature Data

To calculate the membrane protein densities from proteomic data [Fig. S2], we had to compute an empirical description of the surface area as a function of the growth rate. Here, we chose a linear relation that well describes the data with the parameters,

$$S_A = \beta_{S_A,0} + \beta_{S_A,1}\lambda, \tag{14}$$

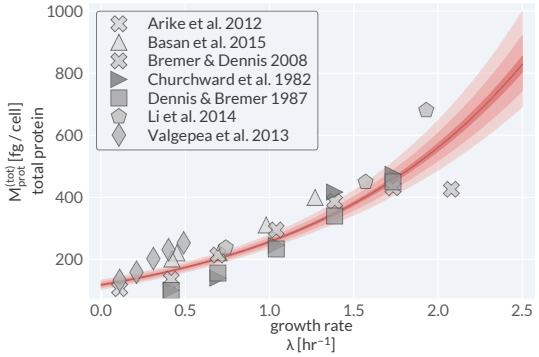

Figure A2: Bayesian fit of total protein per cell as a function of the growth rate. Makers correspond to literature data. Shaded lines denote the bounds of the 95%, 75%, 25%, and median values of the posterior distribution, from light to dark respectively.

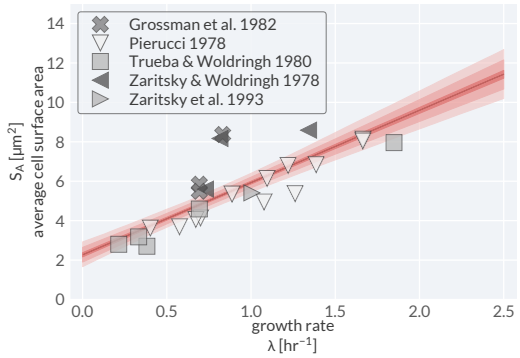

Figure A3: Bayesian fit of average cell surface area as a function of the growth rate. Makers correspond to literature data. Shaded lines denote the bounds of the 95%, 75%, 25%, and median values of the posterior distribution, from light to dark respectively.

which we took to be the mean value of a Gaussian likelihood function (Eq. 11) with a homoskedastic error σ_{S_A}. Precise choices of the prior distributions is provided in Table 1. The result of this fit is shown in Fig. A3.

2.3 Growth Rate Dependent Ribosomal Proteome Fraction from Literature Data

In this work, we present a union between the bacterial "growth laws" which relate cell composition or cell dimension to the steady-state growth rate. Our work presents a predictive theory for the scaling of the surface-to-volume S_A/V with the RNA-to-protein ratio. To evaluate the predicbtive power of our theory, we scoured literature data, but failed to find high-quality measurements of these two quantities made simulataneously. As the ribosomal growth law [Fig. 1(A) of the main text] is well characterized and well understood, we used an empirical fit of this relation to infer the most-likely ribosomal content (and therefore, the RNA-to-protein ratio as described by Eq. 4) for literature data of S_A/V which reported the steady-state growth rate.

To do so, we performed a Bayesian linear regression of the ribosomal proteome fraction ϕ_{rib} as a function of the growth rate λ with the form

$$\phi_{rib} = \beta_{\phi_{rib},0} + \beta_{\phi_{rib},1}\lambda, \tag{15}$$

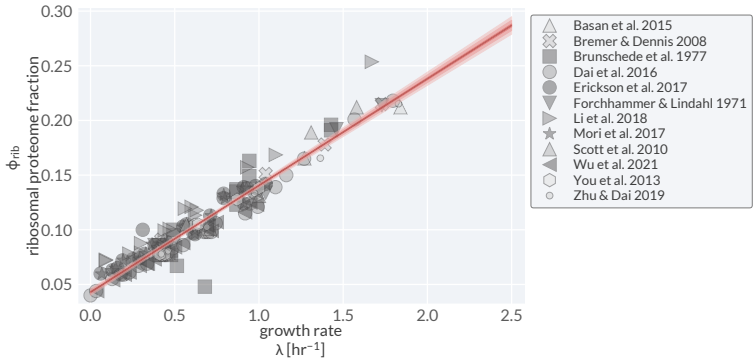

Figure A4: Bayesian fit of ribosomal content as a function of the growth rate. Makers correspond to literature data. Shaded lines denote the bounds of the 95%, 75%, 25%, and median values of the posterior distribution, from light to dark respectively.

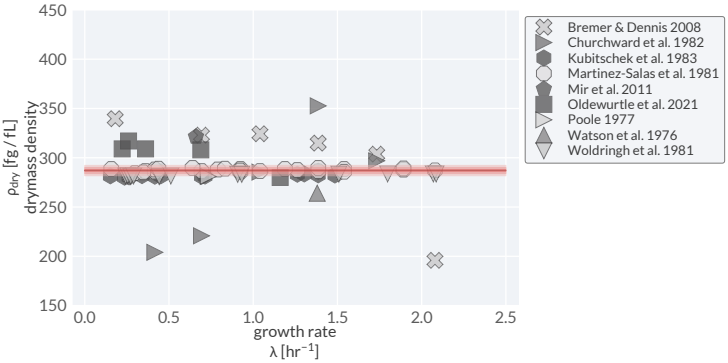

Figure A5: Bayesian fit of total drymass density as a constant. Makers correspond to literature data. Shaded lines denote the bounds of the 95%, 75%, 25%, and median values of the posterior distribution, from light to dark respectively.

which we took to be the mean value of a Gaussian likelihood function (Eq. 11) with a homoskedastic error $\sigma_{\phi_{rib}}$. Precise choices of the prior distributions is provided in Table 1. The result of this fit is shown in Fig. A4.

2.4 Growth-Rate Independent Inference of Total Drymass Density from Literature Data

In this work, we make the well-justified assumption that the total drymass density is independent of the growth rate. As is outlined in Section 1, we further assume this is approximately equal to the cytoplasmic drymass density. To infer this value, we assumed that the drymass density was distributed about a mean $\mu_{drymass}$ with a homoskedastic error $\sigma_{drymass}$, with specific prior distributions outlined in Table 1. The result of this fit is shown in Fig. A5

2.5 Growth-Rate Independent Inference of Membrane Proteome Fraction from Literature Data

A key aspect of the density maintenance theory is that the membrane protein proteome fraction is held at a constant value and is independent of the cell composition as a whole, and thus independent of the growth rate. To infer this value, we assumed that the membrane protein proteome fraction was distributed about

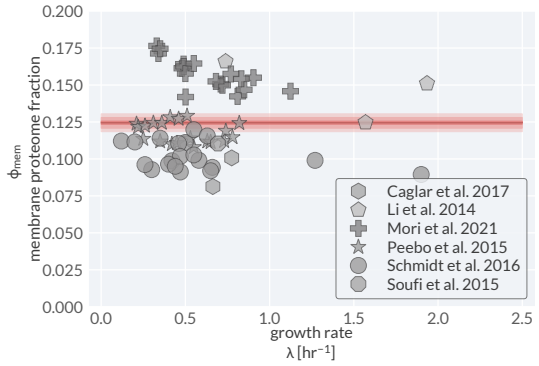

Figure A6: Bayesian fit of membrane proteome fraction as a constant. Makers correspond to literature data. Shaded lines denote the bounds of the 95%, 75%, 25%, and median values of the posterior distribution, from light to dark respectively.

a mean $\mu_{\phi_{mem}}$ with a homoskedastic error $\sigma_{\phi_{mem}}$, whose specific value prior choices are presented in Table. 1. The result of this inference is shown in Fig. A6.

2.6 Growth-Rate Independent Inference of Membrane Protein Density From Literature Data

To our knowledge, there is no comprehensive data set in the literature which directly measures (or infers) the membrane protein areal density as a function of the growth rate across conditions. Thus, we must infer this from other datasets, such as measurement of the membrane protein proteome fraction from proteomic data and empirical measurements of the cell surface area across conditions.

To infer the membrane protein areal density σ_{mem}, we note that this quantity can be computed as

$$\sigma_{mem} = \frac{\phi_{mem} M_{prot}^{(tot)}}{2 S_A}, \tag{16}$$

where $M_{prot}^{(tot)}$ is the total protein mass per cell aned S_A is the average cellular surface area. As demonstrated in the Sec. 2.1 and Sec. 2.2, we have empirical descriptions of these quantities as a function of the growth rate. Futhermore, as we have direct measurements of ϕ_{mem} from various proteomic data sets (Sec. 2.5), we can state that by Eq. 16, ϕ_{mem} can be calculated as

$$\phi_{mem} = \frac{2\sigma_{mem} S_A}{M_{prot}^{(tot)}}. \tag{17}$$

In our inferential approach, we assumed that measurements of ϕ_{mem} were normally distributed about Eq. 17 with a homoskedastic error $\sigma_{phi_{mem}}$. Prior choices for σ_{mem} and $\sigma_{\phi_{mem}}$ are enumerated in Table 1 and the result of this inference, overlaid with the calculated membrane protein densities as described in Fig. S2, are shown in Fig. A7. We note that the density ratio κ used in this work was then calculated as the ratio

$$\kappa = \frac{\mu_{drymass}}{\mu_{\sigma_{mem}}}, \tag{18}$$

using the notation defined in Table 1.

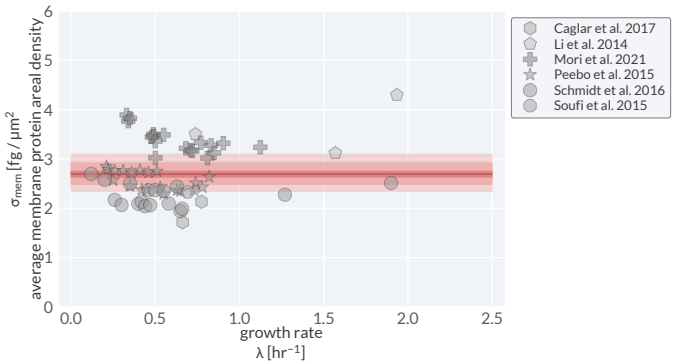

Figure A7: Bayesian fit of membrane protein density fraction as a constant. Makers correspond to literature data. Shaded lines denote the bounds of the 95%, 75%, 25%, and median values of the posterior distribution, from light to dark respectively.

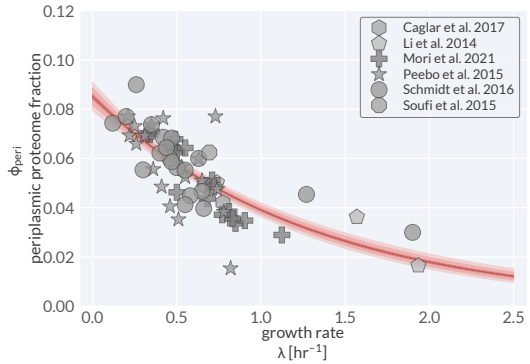

Figure A8: Bayesian fit of periplasmic proteome fraction as a constant periplasmic pass. Makers correspond to literature data. Shaded lines denote the bounds of the 95%, 75%, 25%, and median values of the posterior distribution, from light to dark respectively.

2.7 Growth-Rate Dependent Inference of Periplasmic Proteome Fraction From Literature Data

In addition to the membrane protein proteome fraction parameter ϕ_{mem}, the periplasmic proteome fraction ϕ_{peri} is an important component in calculating the surface-to-volume S_A/V. Unlike ϕ_{mem}, however, this quantity is *not* constant and does appear to have a dependence on the bulk growth rate. Interestingly, we identified using proteomic data that this dependence, coupled with an empirical description of the total protein per cell (Sec. 2.1) resulted in an apparently constant *mass* of periplasmic protein per cell [Fig. S4(B)]. Assuming this is the case, we note that the periplasmic proteome fraction ϕ_{peri} could then be computed as

$$\phi_{peri} = \frac{m_{peri}}{M_{prot}^{(tot)}}, \tag{19}$$

where $M_{prot}^{(tot)}$ denotes the total protein mass per cell as described in Sec. 2.1. We thus assumed that proteomic data measurements of ϕ_{peri} would be Gaussian destributed about a mean defined by Eq. 19 with a homoskedastic error $\sigma_{\phi_{peri}}$ and m_{peri} as a parameter. Specific prior distributions assumed for these parameters are provided in Table 1 and the result from this fit is shown in Fig. A8.

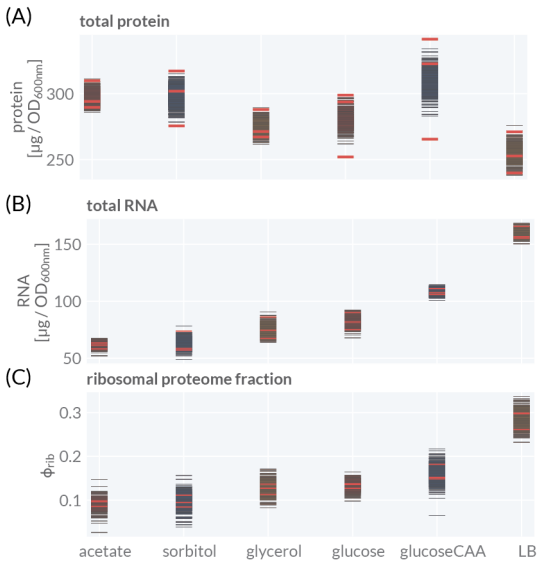

Figure A9: Posterior predictive checks for inference of total RNA, total protein, and ribosomal proteome fractions from our experimental measurement. Black horizontal lines denote draws from the posterior predictive distribution. Red horizontal lines correspond to observed experimental measurements.

2.8 Inference of RNA-to-Protein From Our Experimental Measurements

As described in detail in Sec. 3.2, we experimentally determined the total RNA and total protein mass of *E. coli* cell cultures growing in various conditions. These experiments were preformed in triplicates, meaning that for each growth condition, we had three independent measurements of the RNA-to-protein ratio. We applied a Bayesian inferential model that assumed that measurements of total protein per OD_{600nm}, total RNA per OD_{600nm}, and their ratios were normally distributed about a mean μ each with a homoskedastic error σ and with the specific prior choices as defined in Table. 1. To ensure this model was correctly describing the data generating process, we computed the posterior predictive checks which are simulated experimental draws from a distribution that are conditioned on experimental measurements (Fig. A9). We found that our experimental measurements (red lines) overlapped well with the posterior predictive distributions (black lines).

2.9 Inference of Membrane and Periplasmic Protein From Our Experimental Measurements

In this work, we developed and employed experimental methods to measure the total periplasmic protein and total membrane protein mass for *E. coli* cultures grown in various conditions. These protocols, described in Secs. 3.3.1 and 3.4, respectively, result in biologically independent measurements of the total masses per OD_{600nm} unit. To infer these values, we assumed each set of biological measurements to be drawn from a Gaussian distribution with a mean μ and a homoskedastic error σ. We prescribe the precise prior distributions chosen in Table 1 and show the experimental measurements (red) overlaid with the posterior predictive check distributions (black lines) in Fig. A10, as described in Sec. 2.8.

Figure A10: Posterior predictive checks for inference of total periplasmic and total membrane proteins from our experimental measurements. Black horizontal lines denote draws from the posterior predictive distribution. Red horizontal lines correspond to observed experimental measurements.

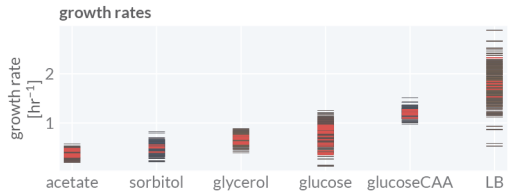

Figure A11: Posterior predictive checks for inference of average growth rates in each condition from experimental measurements. Black horizontal lines denote draws from the posterior predictive distribution. Red horizontal lines correspond to observed experimental measurements.

2.10 Inference of Steady-State Growth Rates From Our Experimental Measurements

For each experiment, we directly measured the growth kinetics of each sample in each condition, resulting in a large collection of growth curves. We restricted each growth curve to the linear regime of our spectrophotometer (determined independently to be between 0.04 and 0.5 OD_{600nm} units) and performed an ordinary linear least squares regression on the log-transformed optical density measurements (not employing a Bayesian approach). To infer the average growth rate of *E. coli* in each growth condition, we compiled the inferred slope from each *individual* growth curve in that condition and assumed they represented draws from a Gaussian distribution with a mean μ and a homoskedastic error σ. Specific prior choices for these parameters are provided in Table 1. We ensured that this model accurately captured the data-generating process by comparing our experimental measurements (red lines) with draws from the posterior predictive distributions (black lines) as shown in Fig. A11.

2.11 Inference of Cell Shape Parameters From Our Experimental Measurements

In addition to biochemical measurements, we directly measured cell size characteristics from microscopy images. Using the average shape parameters from each biological replicate (image processing procedure described in Sec. 4), we again employed a Bayesian model to infer the average values. For each shape property, we assumed that per-replicate averages of width, length, volume, surface area, surface-to-volume, and the aspect ratio were normally distributed about a mean μ and a homoskedastic error σ for each parameter (Table 1). As described in Sec. 2.8, we confirmed we were adequately modeling the data generating process by comparing experimental measurements (red lines) with draws from the posterior predictive distribution (black lines) as shown in Fig. A12.

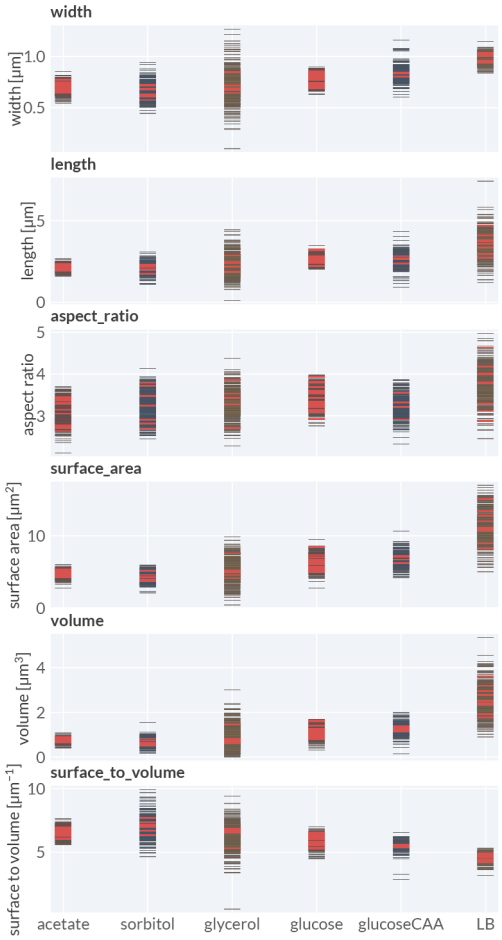

Figure A12: Posterior predictive checks for inference of average cell size parameters in each condition from experimental measurements. Black horizontal lines denote draws from the posterior predictive distribution. Red horizontal lines correspond to observed experimental measurements.

Parameter	Description	Prior(parameters)
$\mu_{\phi_{mem}}$	Average membrane proteome fraction	Beta($\alpha = 2.5, \beta = 8.5$)
$\mu_{\sigma_{mem}}$	Average membrane protein areal density	HalfNormal($\sigma = 1$)
$\sigma_{\phi_{mem}}$	Average membrane proteome fraction homoskedastic error	HalfNormal($\sigma = 0.1$)
$\mu_{\sigma_{mem}}$	Average membrane protein density	HalfNormal($\sigma = 1$)
$\mu_{m_{peri}}$	Average periplasmic protein mass	HalfNormal($\sigma = 10$)
$\sigma_{\phi_{peri}}$	Average periplasmic proteome fraction homoskedastic error	HalfNormal($\sigma = 0.1$)
$\mu_{drymass}$	Average drymass density	Normal($\mu = 300, \sigma = 20$)
$\sigma_{drymass}$	Average drymass homoskedastic error	HalfNormal($\sigma = 10$)
$\mu_{\alpha,0}$	Average aspect ratio (1 subtracted)	HalfNormal($\mu = 0, \sigma = 3$)
σ_{α}	Average aspect ratio homoskedastic error	HalfNormal($\sigma = 1$)
$\beta_{prot,0}$	Log minimal protein per cell	HalfNormal($\sigma = 1$)
k_{prot}	Protein per cell increase per growth rate	Normal($\mu = 3, \sigma = 2$)
$\sigma_{M_{prot}^{(tot)}}$	Log protein per cell homoskedastic error	HalfNormal($\mu = 0, \sigma = 0.1$)
$\beta_{\phi_{rib,0}}$	Ribosomal proteome fraction linear intercept	HalfNormal($\sigma = 0.1$)
$\beta_{\phi_{rib,1}}$	Ribosomal proteome fraction linear slope	HalfNormal($\sigma = 1$)
$\sigma_{\phi_{rib}}$	Ribosomal proteome fraction homoskedastic error	HalfNormal($\sigma = 1$)
$\beta_{S_A,0}$	Average surface area linear intercept	HalfNormal($\sigma = 3$)
$\beta_{S_A,1}$	Average surface area linear slope	HalfNormal($\sigma = 2$)
σ_{S_A}	Average surface area homoskedastic error	HalfNormal($\sigma = 1$)
μ_{prot}	Average protein mass (µg) per OD_{600nm}	HalfNormal($\sigma = 300$)
σ_{prot}	Average protein mass (µg) per OD_{600nm} homoskedastic error	HalfNormal($\sigma = 1$)
μ_{RNA}	Average RNA mass (µg) per OD_{600nm}	HalfNormal($\sigma = 200$)
σ_{RNA}	Average protein mass (µg) per OD_{600nm} homoskedastic error	HalfNormal($\sigma = 1$)
$\mu_{experimental_{\phi_{rib}}}$	Average ribosomal proteome fraction for experimental data	Beta($\alpha = 2.5, \beta = 8.5$)
$\sigma_{experimental_{\phi_{rib}}}$	Average ribosomal proteome fraction for experimental data homoskedastic error	HalfNormal($\sigma = 0.01$)
μ_{peri}	Average periplasmic protein mass (µg) per OD_{600nm}	HalfNormal($\sigma = 100$)
σ_{peri}	Average periplasmic protein mass (µg) per OD_{600nm} homoskedastic error	HalfNormal($\sigma = 10$)
μ_{mem}	Average membrane protein mass (µg) per OD_{600nm}	HalfNormal($\sigma = 20$)
σ_{mem}	Average membrane protein mass (µg) per OD_{600nm} homoskedastic error	HalfNormal($\sigma = 1$)
μ_{λ}	Average growth rate (hr^{-1}) for each experimental condition	HalfNormal($\sigma = 1$)
σ_{λ}	Average growth rate (hr^{-1}) homoskedastic error for each experimental condition	HalfNormal($\sigma = 1$)
μ_{w}	Average cell width (µm) for each experimental condition	HalfNormal($\sigma = 1$)
σ_{w}	Average cell width (µm) homoskedastic error for each experimental condition	HalfNormal($\sigma = 0.5$)
μ_{ℓ}	Average cell length (µm) for each experimental condition	HalfNormal($\sigma = 3$)
σ_{ℓ}	Average cell length (µm) homoskedastic error for each experimental condition	HalfNormal($\sigma = 1$)
μ_{V}	Average cell volume (μm^3) for each experimental condition	HalfNormal($\sigma = 3$)
σ_{V}	Average cell volume (μm^3) homoskedastic error for each experimental condition	HalfNormal($\sigma = 0.5$)
μ_{α}	Average cell aspect ratio (one-subtracted) for each experimental condition	HalfNormal($\sigma = 1$)
σ_{α}	Average cell aspect ratio homoskedastic error for each experimental condition	HalfNormal($\sigma = 0.1$)
μ_{S_A}	Average cell surface area (μm^2) for each experimental condition	HalfNormal($\sigma = 3$)
σ_{S_A}	Average cell surface area (μm^2 homoskedastic error for each experimental condition	HalfNormal($\sigma = 1$)
$\mu_{S_A/V}$	Average cell surface-to-volume (μm^{-1}) for each experimental condition	HalfNormal($\sigma = 3$)
$\sigma_{S_A/V}$	Average cell surface-to-volume (μm^{-1}) homoskedastic error for each experimental condition	HalfNormal($\sigma = 1$)

Table 1: Prior distribution choices for each parameter inferred in this work.

Strain	Source	Description
NCM3722	Laboratory of Terence Hwa	WT
GE463	Plasmid from Addgene, AddGeneID:175594	pMeshI
GE462	Plasmid from Addgene, AddGeneID:175595	pRelA

Table 2: Strains used in this study.

3 Culturing Media and Biochemical assays

3.1 Culturing media

Cultures were grown in Miller LB medium (Fisher Scientific BP1426) or a minimal media, commonly reffered to N-C-. The recipe for the latter is provided on the GitHub repository (`github.com/cremerlab/density_maintenance`). It contains buffer salts (1 g K_2SO_4, 13.5 g K_2HPO_4, 4.7 g KH_2PO_4, 2.5g NaCl, and 0.4 mmol $MgSO_4$ dissolved in water to a volume of 1 liter) which are supplemented with NH_4Cl as nitrogen source (10mM concentration). As carbon sources glucose, glycerol, sodium acetate, or sorbitol were added to the minimal media (with a concentration of 10mM, 20mM, 30mM, or 10mM respectively). Alternatively, glucose and casamino acids were both added as carbon sources (0.1%w/v and 10mM final concentration). Minimal media was freshly prepared on the day of experimentation from a filter-sterilized 4x stock of the buffer salts and by adding NH_4Cl and a selected carbon source from filter-sterilized stock solutions. When needed, antibiotics or inducers were added as described in the Methods.

3.2 Quantification of Total Protein and Total RNA

To quantify total protein in culture samples, we used the well-established biuret method [18] optimized for small sample sizes. The protocol is provided in the following with a step-by-step guideline version further provided on the GitHub repository (`github.com/cremerlab/density_maintenance`). To start, OD_{600nm} of the culture was measured and 1 mL of culture volume was collected from a steadily growing culture ($\approx OD_{600}0.4 - 0.5$). Cells were then harvested via centrifugation, the obtained cell pellet was washed with water, the pellet was re-suspended in 0.2 ml water, and the sample was fast-frozen on dry ice for temporary storage. To quantify protein content, the sample was subsequently thawed at room temperature, 0.1 ml 3M NaOH was added to the sample tube, and the tube was incubated at 100°C to hydrolyze the cells. Samples were then cooled in a water bath at room temperature for 5 min and the biuret reaction was carried out by adding 0.1 ml 1.6% $CuSO_4$ to the sample tube and waiting for 5 min. The sample was then centrifuged (13k RPM for 3 minutes) and absorbance is measured at a wavelength of 555 nm. To obtain a standard curve, the same steps are also replied to a series of BSA concentrations (0, 25, 50, 125, 250, 500, 750, 1000, 1500, 2000 µg/mL). If not stated, centrifugation was run at 13k RPM for 1 minute. For the quantification of cytoplasmic proteins, the same steps were followed but the cell pellet from the periplasmic protein extraction protocol was used as a starting point.

To quantify the total RNA content we used a classical perchloric acid assay [19]. The protocol is provided in the following with a step-by-step guideline version further provided on the GitHub repository (`github.com/cremerlab/density_maintenance`). To start, 1.5 mL sample volume was transferred from a cell culture into a 2 mL microtube, cells were collected via centrifugation and suqsequent supernatant removal, and tubes were put on dry ice. Next, cells were washed twice with 600 µL cold 0.7M $HClO_4$, and cells were digested with 300 µL 0.3M KOH for 60 minutes at 37C. 100µL 3M $HClO_4$ was next added to the extracts, followed by a centrifugation step and the collection of 400µL supernatant into a new 2 mL collection microtube. The remaining precipitate was washed twice with 550µL cold 0.5M $HClO_4$. Each time the supernatant was added to the collection tube. The 1.5 mL liquid in the collection tube was the centrifuged to spin down any remaining precipitates and the OD_{260nm} of the supernatant was measured with a UV-Vis spectroscope (Thermo Genesys 10S). The RNA amount follows as $R(\mu g/ml/OD_{600}) = OD_{260} * 31/OD_{600}$.

To account for cell loss during washing steps, OD_{600nm} of all supernatants were measured and the initial culture OD_{600nm} was corrected accordingly.

3.3 Quantification of Total Periplasmic Protein

3.3.1 Overview and Control

To quantify periplasmic protein mass, we adopted a previously used protein separation assay [20]. The assay is outlined in Figure A13(A). It works by exposing cells to a sucrose solution followed by a mild osmotic shock such that the outer membrane becomes leaky and periplasmic proteins escape into the surrounding solution. Periplasmic proteins are then separated from cytoplasmic and membrane proteins by centrifugation with the periplasmic protein fraction remaining in the supernatant. The protein mass of the supernatant is then quantified via a total protein assay. We optimized the protocol to require small sample volumes and use a protein quantification assay compatible with the separation steps. The protocol is provided in the following with a step-by-step guideline version further provided on the GitHub repository (`github.com/cremerlab/density_maintenance`). As control, we further quantified the enrichment of different proteins in the periplasmic protein fraction using mass spectrometry (experimental details below). The results show that the separation assay works well. First, as expected, most of the periplasmic proteins are highly enriched in the periplasmic protein fraction compared to a total protein sample (no separation), while the relative abundance of most other proteins was substantially lower in the periplasmic protein fraction.[Figure A13(B)].

3.3.2 Separation Protocol

To start, the density (OD_{600nm}) of the culture was measured and 1 ml culture volume was transferred to a 2 ml microtube. A cell pellet was obtained via centrifugation which was then washed with 400 µL PBS at pH 7.4 (NaCl 137 mM, KCl 2.7 mM, Na_2HPO_4 24.2 mM, KH_2PO_4 5.2 mM). After centrifugation and the careful removal of the supernatant, the cell pellet was then resuspended in 400 µL of spheroplast buffer (0.1 M Tris pH 8.0, 500 mM sucrose, 0.5 mM EDTA pH 8.0) and incubated for 5 min on ice. Next, the sample was centrifuged again, and the supernatant was discarded. Cells were then subjected to an osmotic shock by resuspending the pellet in 400 µL hypotonic solution of 1mM MgCl2 with a 2-minute incubation on ice following. After centrifugation, the supernatant was carefully transferred to a new microtube. Periplasmic proteins mass in the supernatant was immediately quantified via the Bradford assay using the Bio-Rad protein assay kit (catalog number 5000002) and following the instructions for the micro assay protocol. Specifically, 800 µL of protein sample was mixed with 200 µL of the Bradford dye solution and absorbance was measured at a wavelength of 595 nm. Standard curves were generated using BSA and IgG over the concentration ranges mentioned in the manual. All centrifugation steps were carried out with a bench top centrifuge at 4C, 8000 rpm, and for a duration of 8 min.

3.3.3 Mass Spectrometry to Confirm Separation Assay

The proteome samples were collected after the separation procedure depicted in Fig. A13(A) and as described above. Proteins were denatured and reduced with 1% SDS and beta-mercaptoethanol at 95°C for

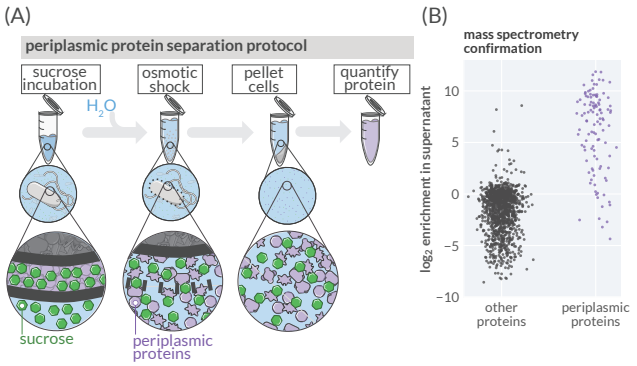

Figure A13: Validation of the periplasmic protein extraction protocol. (A) Periplasmic protein isolation protocol employing sucrose incubation and a mild osmotic shock. (B) Probing separation assay using mass spectrometry. Fold change in relative abundance of detected proteins comparing a periplasmic protein fraction sample with a total protein sample (no separation). Classification into proteins annotated as periplasmic proteins and all others. (C) Fraction of overall detected ion intensity from all proteins classified as periplasmic, ribosomal, or other proteins. Analysis shown for periplasmic protein fraction and total protein (no separation) samples. Samples were taken from a steady state culture (minimal media with acetate as carbon source).

10min (with vortexing). Debris was pelleted by centrifugation for 10 minutes (10,000g). Cleared supernatants were alkylated with 5mM iodoacetamide, and then precipitated with three volumes of a solution containing 50% acetone and 50% ethanol. Proteins were re-solubilized in 2 M urea, 50 mM Tris-HCl, pH 8.0, and 150 mM NaCl, and then digested with TPCK-treated trypsin (50:1) overnight at 37°C. Trifluoroacetic acid and formic acid were added to the digested peptides for a final concentration of 0.2%. Peptides were desalted with a Sep-Pak 50mg C18 column (Waters). The C18 column was conditioned with 500μl of 80% acetonitrile and 0.1% acetic acid and then washed with 1000μl of 0.1% trifluoroacetic acid. After samples were loaded, the column was washed with 2000μl of 0.1% acetic acid followed by elution with $400\mu l$ of 80% acetonitrile and 0.1% acetic acid. The elution was dried in a concentrator at 45°C. De-salted peptides were resuspended in 0.1% formic acid.

Desalted SILAC-labeled peptides were analyzed on a Fusion Lumos mass spectrometer (Thermo Fisher Scientific) equipped with a Thermo EASY-nLC 1200 LC system (Thermo Fisher Scientific). Peptides were separated by capillary reverse phase chromatography on a 25 cm column (75 μm inner diameter, packed with 1.6 μm C18 resin, AUR2-25075C18A, Ionopticks, Victoria Australia). Peptides were introduced into the Fusion Lumos mass spectrometer using a 125 min stepped linear gradient at a flow rate of 300 nL/min. The steps of the gradient are as follows: 3–27% buffer B (0.1% (v/v) formic acid in 80% acetonitrile) for 105 min, 27-40% buffer B for 15 min, 40-95% buffer B for 5min, maintain at 90% buffer B for 5 min. Column temperature was maintained at 50°C throughout the procedure. Xcalibur software (Thermo Fisher Scientific) was used for the data acquisition and the instrument was operated in data-dependent mode. Advanced peak detection was enabled. Survey scans were acquired in the Orbitrap mass analyzer (Profile mode) over the range of 375 to 1500 m/z with a mass resolution of 240,000 (at m/z 200). For MS1, the Normalized AGC Target (%) was set at 250 and max injection time was set to "Auto". Selected ions were fragmented by Higher-energy Collisional Dissociation (HCD) with normalized collision energies set to 31 and the tandem mass spectra was acquired in the Ion trap mass analyzer with the scan rate set to "Turbo". The isolation window was set to 0.7 m/z window. For MS2, the Normalized AGC Target (%) was set to "Standard" and max injection time was set to "Auto". Repeated sequencing of peptides was kept to a minimum by dynamic exclusion of the sequenced peptides for 30 seconds. Maximum duty cycle length was set to 1 second.

All raw files were searched using the Andromeda engine embedded in MaxQuant (v2). Maxquant's LFQ was enabled. Variable modifications included oxidation (M) and protein N-terminal acetylation. Carbamidomthyl (C) was a fixed modification. The number of modifications per peptide was capped at five. Digestion was set to tryptic (proline-blocked). Maxquant's match-between-runs feature was not enabled. Database search was conducted using the UniProt proteome - `Ecoli_UP000000625_83333`. The minimum peptide length was 7 amino acids. 1% FDR was determined using a reverse decoy proteome. Quantified peptides were collated into protein-level ion intensities in Maxquant's "proteinGroups.txt" file.

To approximate the enrichment of periplasmic and ribosomal proteins before and after the enrichment procedure, each protein was first annotated as either a periplasmic, ribosomal, or "other" protein (based on Uniprot annotations). The relative enrichment for each detected protein in the periplasm is shown in Fig. A13(B).

3.4 Quantification of Total Membrane Protein

To quantify membrane protein mass we developed a biochemical assay which in short, combines cell lysis via sonication, ultra-centrifugation to extract membrane proteins. Total protein mass of the obtained membrane fraction is then measured. We have optimized the protocol to work with small culture volumes and to ensure that protein separation and quantification steps are compatible. The protocol is provided in the following with a step-by-step guideline version further provided on the GitHub repository (`github.com/cremerlab/density_maintenance`). To start, 2x 1ml culture volumes were transferred from a steadily growing culture at a density of $OD600 \approx 0.5$ into a 2ml microtube. Cells were collected via standard centrifugation and the subsequent removal of the supernantant. To remove protein from the media, samples from LB cultures were further washed in 1ml of PBS at pH 7.5 (137 mM NaCl, 2.7 mM KCl, 24.2 mM Na_2HPO_4, 5.2 mM KH_2PO_4) with subsequent centrifugation and removal of the supernantant. Samples were frozen at -80C for at least 30 minutes before further processing. For lysis, samples were then thawed at room temperature for 5 minutes, cell pellets were suspended in 500µL of cold spheroplast buffer (0.1 M Tris pH 8.0, 500 mM sucrose, 0.5 mM EDTA pH 8.0), and tubes were incubated on ice for 20 min. Next, 500µL of 100 mM $MgCl_2$ was added and tubes were incubated for an additional 10 minutes. The liquid was then transferred to a 15ml Falcon tube and sonication (Branson Sonicator 450) was run 3 times for an interval of 30-seconds each with 5 second breaks between the runs. After sonication, the liquid was transferred back to the original microtube, followed by centrifugation. The supernatant (approx. 1mL) was then transferred to two ultracentrifugation tubes (Beckman Coulter 8x34mm tubes, catalogue number 343775; approx. 0.5 mL supernatant per tube). To quantify the protein content of unlysed cells, the remaining cell pellet was resuspended in 500µL of 2% SDS, heated at 100° C for 30 min, and quantified via the biuret total protein assay (see Section 3.2). To separate membrane proteins from other proteins, spheroplast buffer was then added to the lighter tube until less than 0.01g difference in weight between both tubes was obtained, arranged on the rotor, and ultra-centrifugation was run for 1h at 4C. Subsequently, the supernatant containing mostly cytoplasmic proteins was carefully removed without touching the pellet. To extract the pellet with membrane proteins, 150µL 2% SDS was immediately added to the UC tubes and the pellet was suspended and mixed via thorough pipetting (30-60 seconds per sample). To quantify protein content we used the Thermo Fisher Micro BCA Protein Assay Kit (catalogue number 23235) following the provided instructions and using a BioTek Epoch2 microplate reader set for incubation at 37C. Specifically per sample,

150µL of the supernatant was transferred to a well of a 96-well microtiter plate (Greiner CELLSTAR 655 185). To start the reaction, 150µL of working reagent were then added to each well and the plate was transferred to the plate reader. After 30 seconds of shaking, incubation was continued for 2h without shaking before absorbance readings at a wavelength of 562nm were taken. To generate a standard curve samples with different BSA concentrations were taken following the same protocol and concentrations were calculated comparing absorbance reading and accounting for culture dilutions. Standard centrifugation steps were carried out with a bench top centrifuge at 4°C with a speed of 8000 rpm, and for a duration of 2 min. Ultra-centrifugation was carried out with a Beckman Coulter OptimaMAX ultracentrifuge at 4°C with rotor Beckman Coulter TLA-120.1 at a speed of 65k rpm.

4 Image Processing

In this work, we directly measured cell size parameters from phase-contrast microscopy images at 100X magnification. We employed an in-house image processing Python pipeline to segment and measure per-cell parameters. The steps of this segmentation algorithm are outlined in Fig. A14. Briefly, individual cells are identified in an image through several rounds of filtering and thresholding. Once cell masks are identified, each is rotated and aligned to a common axis and contours are determined by edge detection, smoothing, and spline interpolation. With a spline interpolation in place, the curvature k along the contour along an xy coordinate system at each point is calculated via

$$k = \frac{x'y'' - y'x''}{(x'^2 + y'^2)^{3/2}} \tag{20}$$

Note that this preserves sign of the curvature. By rotating each cell mask to have the same axis of orientation, we can ensure that the sign of the curvature is consistent between individual cells and images.

With an estimate of the cell curvature in place at each position along the contour, we apply a threshold on this value to identify what portions of the contour correspond to the cell sides ($k \approx 0$) versus the cell caps ($|k| > 0$). We identified the cap regions of the cells as the contour points with radii of curvature greater than 0.5 µm. To compute the cell length dimension, we took the length to be the maximum y coordinate difference between contour points of the two caps. For the width, we computed the average minimum pairwise distance between the two cell side contours. Representative segmented cell peripheries are shown in Fig. A15 for 60 cells from a single image. We found that our segmentation protocols yielded measurements that were in line with literature cell size measurements and exhibited the same apparent growth-rate dependence, as shown in Fig. A16

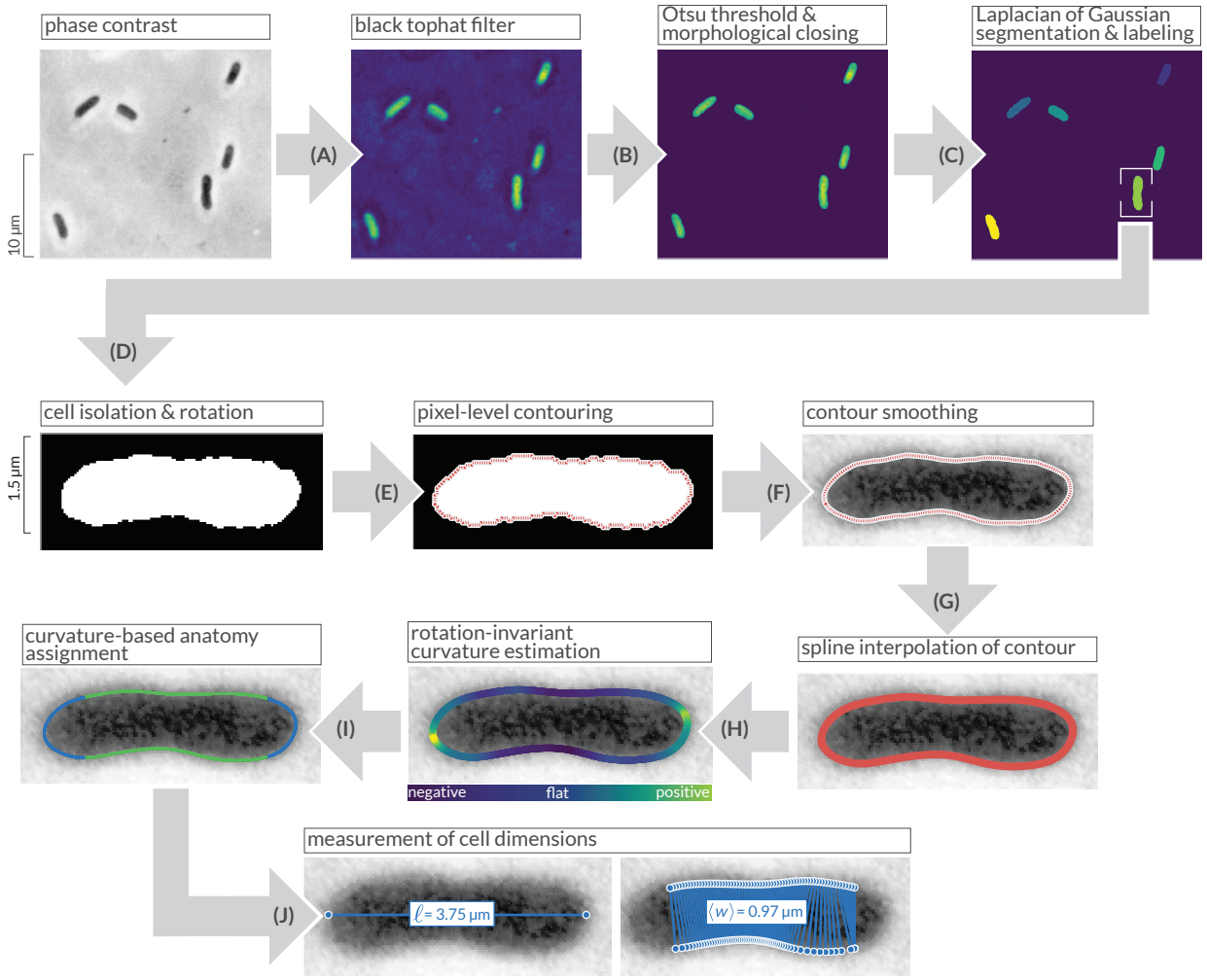

Figure A14: Segmentation and cell measurement pipeline. Raw phase-contrast images of cells are passed through (A) a black tophat filter and (B) Otsu thresholding to arrive at emphasized cell boundaries. (C) Laplacian of Gaussian segmentation is then applied to arrive at rough cell masks. For each cell, the sgementation mas is (D) rotated and aligned and the periphery is identified using (E) contouring and (F) Savgol filtering. The isolated contours are then smoothed with (G) spline interpolation. In a clock-wise direction, the (H) curvature of the contour is calculated and used to (I) identify sides and caps. With morphology assigned, cell dimensions are then (J) measured.

Figure A15: Example segmentation of *E. coli* cells grown steadily on a glucose and casamino acid supplemented minimal medium. Blue and green regions of the contours correspond to the caps and sides of the cells, respectively.

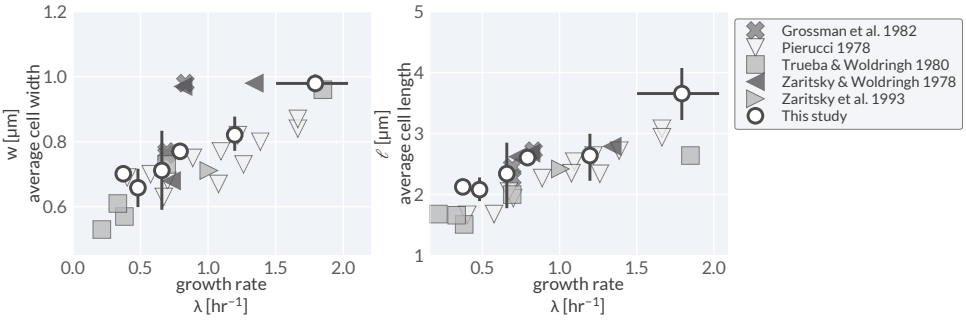

Figure A16: Comparison of our size measurements with literature data. White-faced points correspond to measurements from this study. Error bars denote bounds of the 95% credible region of the posterior parameter estimate.

.

References

[1] Hans Bremer and Patrick P. Dennis. Modulation of Chemical Composition and Other Parameters of the Cell at Different Exponential Growth Rates. *EcoSal Plus*, 3(1), October 2008. Publisher: American Society for Microbiology.

[2] Alexander Schmidt, Karl Kochanowski, Silke Vedelaar, Erik Ahrné, Benjamin Volkmer, Luciano Callipo, Kèvin Knoops, Manuel Bauer, Ruedi Aebersold, and Matthias Heinemann. The quantitative and condition-dependent *Escherichia coli* proteome. *Nature Biotechnology*, 34(1):104–110, January 2016.

[3] Boumediene Soufi, Karsten Krug, Andreas Harst, and Boris Macek. Characterization of the *E. coli* proteome and its modifications during growth and ethanol stress. *Frontiers in Microbiology*, *6*, February 2015. tex.ids: soufi2015a.

[4] Mehmet U. Caglar, John R. Houser, Craig S. Barnhart, Daniel R. Boutz, Sean M. Carroll, Aurko Dasgupta, Walter F. Lenoir, Bartram L. Smith, Viswanadham Sridhara, Dariya K. Sydykova, Drew Vander Wood, Christopher J. Marx, Edward M. Marcotte, Jeffrey E. Barrick, and Claus O. Wilke. The E. coli molecular phenotype under different growth conditions. *Scientific Reports*, 7(1):1–15, April 2017.

[5] Kaspar Valgepea, Kaarel Adamberg, Andrus Seiman, and Raivo Vilu. Escherichia coli achieves faster growth by increasing catalytic and translation rates of proteins. *Molecular BioSystems*, 9(9):2344–2358, July 2013. Publisher: The Royal Society of Chemistry.

[6] Matteo Mori, Zhongge Zhang, Amir Banaei-Esfahani, Jean-Benoît Lalanne, Hiroyuki Okano, Ben C Collins, Alexander Schmidt, Olga T Schubert, Deok-Sun Lee, Gene-Wei Li, Ruedi Aebersold, Terence Hwa, and Christina Ludwig. From coarse to fine: the absolute *Escherichia coli* proteome under diverse growth conditions. *Molecular Systems Biology*, 17(5), May 2021.

[7] Gene-Wei Li, David Burkhardt, Carol Gross, and Jonathan S. Weissman. Quantifying absolute protein synthesis rates reveals principles underlying allocation of cellular resources. *Cell*, 157(3):624–635, April 2014.

[8] Markus Basan, Manlu Zhu, Xiongfeng Dai, Mya Warren, Daniel Sévin, Yi-Ping Wang, and Terence Hwa. Inflating bacterial cells by increased protein synthesis. *Molecular Systems Biology*, 11(10):836, October 2015. Publisher: John Wiley & Sons, Ltd.

[9] Gordon Churchward, Hans Bremer, and Ry Young. Macromolecular composition of bacteria. *Journal of Theoretical Biology*, 94(3):651–670, February 1982.

[10] Jes Forchhammer and Lasse Lindahl. Growth rate of polypeptide chains as a function of the cell growth rate in a mutant of Escherichia coli. *Journal of Molecular Biology*, 55(3):563–568, February 1971.

[11] Mohan Babu, Cedoljub Bundalovic-Torma, Charles Calmettes, Sadhna Phanse, Qingzhou Zhang, Yue Jiang, Zoran Minic, Sunyoung Kim, Jitender Mehla, Alla Gagarinova, Irina Rodionova, Ashwani Kumar, Hongbo Guo, Olga Kagan, Oxana Pogoutse, Hiroyuki Aoki, Viktor Deineko, J. Harry Caufield, Erik Holtzapple, Zhongge Zhang, Ake Vastermark, Yogee Pandya, Christine Chieh-lin Lai, Majida

El Bakkouri, Yogesh Hooda, Megha Shah, Dan Burnside, Mohsen Hooshyar, James Vlasblom, Sessandra V. Rajagopala, Ashkan Golshani, Stefan Wuchty, Jack F Greenblatt, Milton Saier, Peter Uetz, Trevor F Moraes, John Parkinson, and Andrew Emili. Global landscape of cell envelope protein complexes in Escherichia coli. *Nature Biotechnology*, 36(1):103–112, January 2018. Number: 1 Publisher: Nature Publishing Group.

[12] L. Arike, K. Valgepea, L. Peil, R. Nahku, K. Adamberg, and R. Vilu. Comparison and applications of label-free absolute proteome quantification methods on Escherichia coli. *Journal of Proteomics*, 75(17):5437–5448, September 2012.

[13] H Bremer and Patrick P. Dennis. *Modulation of chemical composition and other parameters of the cell by growth rate. Neidhardt, et al. eds. Escherichia coli and Salmonella typhimurium: Cellular and Molecular Biology, 1st ed. chapter 96, Table 2 pp.1530-1*. Escherichia coli and Salmonella typhimurium: Cellular and Molecular Biology,. 1 edition, 1987.

[14] Ron Milo, Paul Jorgensen, Uri Moran, Griffin Weber, and Michael Springer. BioNumbers—the database of key numbers in molecular and cell biology. *Nucleic Acids Research*, 38(suppl_1):D750–D753, January 2010. tex.pmcid: [object Object] tex.pmid: [object Object].

[15] Matthew Scott, Carl W. Gunderson, Eduard M. Mateescu, Zhongge Zhang, and Terence Hwa. Interdependence of Cell Growth and Gene Expression: Origins and Consequences. *Science*, 330(6007):1099–1102, November 2010. tex.ids: scott2010a Publisher: American Association for the Advancement of Science Section: Report.

[16] Abir T. Asmar, Josie L. Ferreira, Eli J. Cohen, Seung-Hyun Cho, Morgan Beeby, Kelly T. Hughes, and Jean-François Collet. Communication across the bacterial cell envelope depends on the size of the periplasm. *PLOS Biology*, 15(12):e2004303, December 2017. Publisher: Public Library of Science.

[17] Bob Carpenter, Andrew Gelman, Matthew D. Hoffman, Daniel Lee, Ben Goodrich, Michael Betancourt, Marcus Brubaker, Jiqiang Guo, Peter Li, and Allen Riddell. Stan: A probabilistic programming language. *Journal of Statistical Software*, 76(1):1–32, January 2017.

[18] D. Herbert, P.J. Phipps, and R.E. Strange. Chapter iii chemical analysis of microbial cells. volume 5 of *Methods in Microbiology*, pages 209–344. Academic Press, 1971.

[19] S. Benthin, J. Nielsen, and J. Villadsen. A simple and reliable method for the determination of cellular rna content. *Biotechnology Techniques*, 5(1):39–42, Jan 1991.

[20] Gilles Malherbe, David Paul Humphreys, and Emma Davé. A robust fractionation method for protein subcellular localization studies in *Escherichia coli*. *BioTechniques*, 66(4):171–178, April 2019.